catalysts

MDPI

Article

Low-Cost Synthesis of Cu-Modified Immobilized Nanoporous TiO_2 for Photocatalytic Degradation of 1H-Benzotriazole

Tihana Čižmar [1], Ivana Panžić [1], Krešimir Salamon [1], Ivana Grčić [2], Lucija Radetić [2], Jan Marčec [2] and Andreja Gajović [1,*]

1 Ruđer Bošković Institute, Bijenička 54, HR-10000 Zagreb, Croatia; tcizmar@irb.hr (T.Č.); ipanzic@irb.hr (I.P.); kresimir.salamon@irb.hr (K.S.)

2 Faculty of Geotechnical Engineering, University of Zagreb, Hallerova Aleja 7, HR-42000 Varaždin, Croatia; igrcic@gfv.hr (I.G.); lucija.radetic@gfv.hr (L.R.); jan.marcec@gfv.hr (J.M.)

* Correspondence: gajovic@irb.hr

Received: 31 October 2019; Accepted: 16 December 2019; Published: 21 December 2019

Abstract: Cu-modified immobilized nanoporous TiO_2 photocatalysts, prepared by electrochemical anodization of titanium foils, were obtained via four different synthesis methods: hydrothermal synthesis, anodization with Cu source, electrodeposition, and spin-coating, using two different copper sources, $Cu(NO_3)_2$ and $Cu(acac)_2$. The objective of this research was to investigate how copper modifications can improve the photocatalytic activity of immobilized nanoporous TiO_2 under the UV/solar light irradiation. The best photocatalytic performances were obtained for Cu-modifications using spin-coating. Therefore, the effect of irradiated catalyst surface areas on the adsorption of model pollutants, methylene blue (MB) and 1H-benzotriazole (BT), was examined for samples with Cu-modification by the spin-coating technique. The mechanisms responsible for increased degradation of MB and BT at high Cu concentrations (0.25 M and 0.5 M) and decreased degradation at low Cu loadings (0.0625 M and 0.125 M) were explained. 1H-benzotriazole was used to study the photocatalytic activity of the given samples because it is highly toxic and present in most water systems. The characterization of the synthesized Cu-modified photocatalysts in terms of phase composition, crystal structure, and morphology were investigated using X-ray Diffraction, Raman Spectroscopy, Scanning Electron Microscopy, and Energy Dispersive X-ray spectroscopy.

Keywords: immobilized nanoporous TiO_2; electrochemical anodization; Cu-modification; photocatalytic activity; spin-coating; 1H-benzotriazole

1. Introduction

Titanium dioxide is chemically stable, non-toxic, commercially available, and it has excellent photocatalytic properties [1–5]. Due to these facts, it has been widely used for the removal of residual pesticides, water purification, degradation of air pollutants, hydrogen production, sensing, etc. [6–11].

When the light is absorbed by the photocatalyst, an electron from the valence band promotes to the conduction band, leaving an electron deficiency or hole (h^+) in the valence band and an excess of negative charge in the conduction band (e^-) which are participating in redox reactions responsible for organics pollutant degradation. Oxidative degradation using TiO_2 can be obtained with two different photocatalytic systems: immobilized TiO_2 and particle suspension [12]. The reuse of photocatalysts presents an important role in the industrial application of the technology; therefore, efficient separation of TiO_2 particles from the treated solution is an essential objective. That is the reason why a great focus has been put to immobilization of TiO_2—to avoid the need for the separation of the photocatalysts from the treated solution.

Synthesis of immobilized nanoporous TiO_2 is a relatively inexpensive, simple, and fast process that can be applied on a large-scale. These vertically aligned TiO_2 nanostructures are grown by electrochemical anodization from a metallic Ti substrate. Dimensions and physical or chemical behavior can easily be controlled by electrochemical parameters [13,14]. Nanoporous TiO_2 has a high specific surface area, large electron mobility, and beneficial charge separation properties that improve photocatalytic activity [13,15].

Despite of the abovementioned advantages, TiO_2 has one major disadvantage: the inability to absorb the visible part of solar spectrum due to its wide bandgap (3.0–3.2 eV); therefore, modifications of TiO_2 photocatalysts that would allow visible light absorption could significantly improve its photocatalytic activity. Moreover, to improve photocatalytic activity under UV/Vis light irradiation, a high recombination rate between photogenerated electrons and holes in TiO_2 needs to be reduced, meaning that more photogenerated electrons and holes could move to the surface of the semiconductor particles before they recombine. Surface modification (decoration of the TiO_2 nanostructures with noble metal particles or metal oxides), metal and non-metal doping, dye sensitization, and semiconductor coupling have been used to improve TiO_2 photocatalytic activity under UV/Vis light irradiation [16–24].

The addition of small amounts of metal cations can reduce high rate recombination between electrons and holes. Modifying or doping TiO_2 with different metals can introduce new electron capture centers or generate additional electronic states in the TiO_2 band gap above the valence band, capturing the photo-formed holes [18,25]. Modification of TiO_2 with noble metal nanoparticles (Pt, Pd, Au, and Ag) restricts the recombination of electron-hole pairs, which leads to enhanced photocatalytic activity. The Fermi level of noble metals is lower than the conduction band (CB) of TiO_2, so when the electrons at the valence band (VB) of TiO_2 are excited by the light irradiation, electrons transfer from the VB of TiO_2 to the CB of TiO_2 and then to the noble metal nanoparticles. Since the Schottky barrier is formed at the junction due to the existence of an internal electric field between TiO_2 and metal nanoparticles, it leads to efficient charge separation and nanoparticle acts as a trap for the generated charge carriers. Simultaneously, the photogenerated holes remain and are involved in the oxidation reactions [15,26–29]. Because noble metals are rare and expensive, copper is a good candidate to replace them. The improved photocatalytic activity was found particularly for TiO_2 modifications with low Cu concentrations [30–32]. Copper nanoparticles (NP), similar to noble metal nanoparticles, are promising surface modifiers of TiO_2 because they restrict the recombination of electron-hole pairs, which leads to enhanced photocatalytic activity both under UV and visible light irradiation. Furthermore, when light interacts with the free electrons of Cu NP, surface plasmon resonance (SPR) is activated. That leads to the collective excitations of the free electrons of Cu metallic nanoparticles, improving the local electromagnetic field surrounding them [33]. Activation towards visible light photocatalytic activity occurs due to the SPR band that absorbs light in the visible region [34–36].

Theoretical simulations [37] indicate that Cu is the most stable when highly dispersed at anatase (101) surface and in a 2+ oxidation state. Electronic interactions facilitated via the mechanism of charge transfer (metal-to-metal charge transfer; Cu–O–Ti connections) increase the lifetime of surface holes and increase the photocatalytic activity through charge carrier separation [38].

A promising way to achieve visible light activation of TiO_2 is surface modification with metal oxide clusters, particularly Cu(II) ions and CuO [19,39–43]. When $Cu(acac)_2$ is used as a precursor in the synthesis, it forms small CuO clusters on the surface of TiO_2 particles in a highly dispersed state. $Cu(acac)_2$ complex could be chemisorbed on TiO_2 via surface Ti−OH groups without the elimination of the acac-ligand. Furthermore, part of the Cu(II) cations may retain bonding to acac-groups as in the crystalline $Cu(acac)_2$ or in the liquid precursor [42].

In this work, the idea is to find simple, low-cost method to improve the photocatalytic activity of TiO_2 nanostructures by broadening the operational conditions of the photocatalyst to work in the visible part of the spectrum. Since it is known from the literature that Cu-based modification of the TiO_2 can improve the photocatalytic activity of TiO_2, we studied four different synthesis methods of TiO_2 modification: hydrothermal synthesis, anodization with Cu source, electrodeposition, and spin-coating.

Therefore, the objective of this research is to study how modification with copper-based compounds can improve the photocatalytic activity of nanoporous TiO_2, and to explain the correlation between different synthesis paths and Cu concentration with the photocatalytic activity under the UV/solar light irradiation. It was shown that samples synthesized with spin-coating and hydrothermal synthesis have similar photocatalytic activity, but spin-coating is faster, cheaper, and more suitable for scale-up and possible commercialization.

1H-benzotriazole was used as a model pollutant since it is a broad applicative but highly toxic compound. It is a complexing agent used as an anticorrosive in fire retardant, antifreeze, and airplane de-icing/anti-icing fluid [44]. Benzotriazoles are well-known environmental contaminants whose presence is detected in most water systems: river streams and even in the groundwater. Used products, which contain benzotriazoles, may leak or be poured down the drain entering the environment. Furthermore, there is a large number of benzotriazoles, even in the sewage system. On the other hand, approximately 80% of aircraft de-icing/anti-icing fluids, which are deposited on the ground due to spray drift, jet blast, and wind shear during taxiing and take-off [45], infiltrate the groundwater.

Recent findings indicated a higher concentration of benzotriazole compounds in the groundwater in comparison to the surface water; therefore, this research was based on studying benzotriazole photocatalytic degradation [46]. Benzotriazoles are prone to photolysis under sunlight, but the reaction is rather slow. In our work, we showed full degradation of 1H-benzotriazole (BT) under the artificial full-spectra solar light irradiation. Results are compared with those obtained for photocatalytic degradation of methylene blue (MB), which was used as a referent model pollutant.

2. Results and Discussion

2.1. Photocatalytic Activity

In the current study, 15 different samples of photocatalytic films were prepared to find an optimal preparation method and the Cu content for the photocatalytic degradation of 1H-benzotriazole (BT). Methylene blue dye (MB) was used as a referent model pollutant. The preparation method for each film and its modification with the Cu-based compounds are given in Table 1, while the details of preparation and explanation of the samples' full names are given in section Materials and methods (see Section 3.1). Sets of samples A–E and sample F3s had a uniform circular surface area of 0.5 cm^2 (D = 0.8 cm), while set F had a larger circular surface area of 2 cm^2 (D = 1.6 cm). The sample A2 was taken as a reference sample (annealed nanoporous TiO_2), and that particular sample was prepared in two surface area sizes, both 0.5 cm^2 (D = 0.8 cm) and 2 cm^2 (D = 1.6 cm) to study the effects of the irradiated area on photocatalytic degradation of pollutants. Sample F3 was also prepared in both surface area sizes. Th first sample (denoted as F3s) is a smaller sample (circular surface area of 0.5 cm^2) used in comparison with samples A–E. Furthermore, the series of samples with the larger surface areas were prepared (F1–F4) to study the influence of different Cu concentration and irradiated areas on the photocatalytic activity. The numerical comparison of photocatalytic activity of TiO_2 nanoparticles prepared by anodization (A2 sample) and commercial TiO_2 (TiO_2 P25) was elaborated in our previous study [29]. Having in mind the specific form of prepared photocatalyst and the inability to produce the film having only pure TiO_2 P25 with similar characteristics, the comparative quantification was done using the numerical method according to the presented algorithm. That way, a comparison was made numerically, using the detailed kinetic model, referent constants for P25 (adsorption and scattering coefficient), and the intrinsic kinetic rates [29]. The study demonstrated the similar photocatalytic activity of TiO_2 NP in each spectral range (UV and visible) as the one expected for commercial TiO_2 P25. The similar is expected here, so the A2 sample was used as a reference for estimation of Cu contribution on the photocatalytic activity. The expected increase of the photocatalytic activity of Cu-based compounds can be considered as an absolute enhancement of degradation rates normally achieved by the commercial catalyst.

Given photocatalytic samples were used in a specially designed photoreactor SPC (see Section 3.2.1.1) to study the photocatalytic degradation of BT and MB under artificial solar irradiation. The degradation kinetics was shown as pseudo-first-order kinetics (Equation (1)).

$$C_i(t) = C_i(0)\, e^{-kt} \quad (1)$$

As shown in Figure 1, observed first-order reaction rate constants range from 0.047 to 0.556 h^{-1} for MB degradation and from 0.031 to 0.48 h^{-1} for BT degradation. This result confirmed the importance of the preparation method and the amount of Cu concentration deposited on the surface of the nanoporous TiO_2 on the observed photocatalytic activity. Sample F3s (0.250 M) showed the highest activity for the degradation of both MB and BT; therefore, we decided to use spin-coating technique and prepare a full set of catalyst samples with different concentrations of Cu-based compounds (0, 0.0625, 0.125, 0.25, and 0.5 M), denoted as A2 (NP TiO_2), F1 (0.0625 M), F2 (0.125 M), F3 (0.250 M), and F4 (0.500 M), respectively, so these films had four times larger surface (2 cm^2; D = 1.6 cm). One must note that a larger surface is directly connected to the higher amount of catalysts in the system in case of evenly distributed films with the uniform depth, as herein. The objective of this research was (i) to study the effect of the irradiated surface size on the adsorption of pollutants on the film surface and increased photocatalytic activity due to higher amount of the catalyst, (ii) to determine appropriate Cu concentration and (iii) to clarify mechanisms responsible for the increased activity of MB and BT degradation at high Cu concentrations, and decreased activity at low Cu loadings.

Adsorption experiments were performed in the dark, using different initial BT and MB concentration (C_0 = 5, 15, 25, 30 mg dm^{-3}). Results were expressed in the form of a modified Langmuir isotherm (Equation (2)).

$$\frac{1}{q_i^S} = \frac{1}{q_{i,\,max}^S} + \frac{1}{K_{L,i} q_{i,\,max}^S C_{e,i}} \quad (2)$$

In the equation, $q^S{}_i$ represents the surface-related adsorbed amount, i.e., the amount of adsorbed pollutant i per surface area of the photocatalytic film (mg cm^{-2}). The $q^S{}_{i,max}$ is the maximum surface coverage that can be easily extrapolated from a linear model. The $K_{L,i}$ is the binding constant (dm^3 mg^{-1}), and the $C_{e,i}$ is the concentration on BT or MB at equilibrium. Langmuir isotherms are shown in Figure 2.

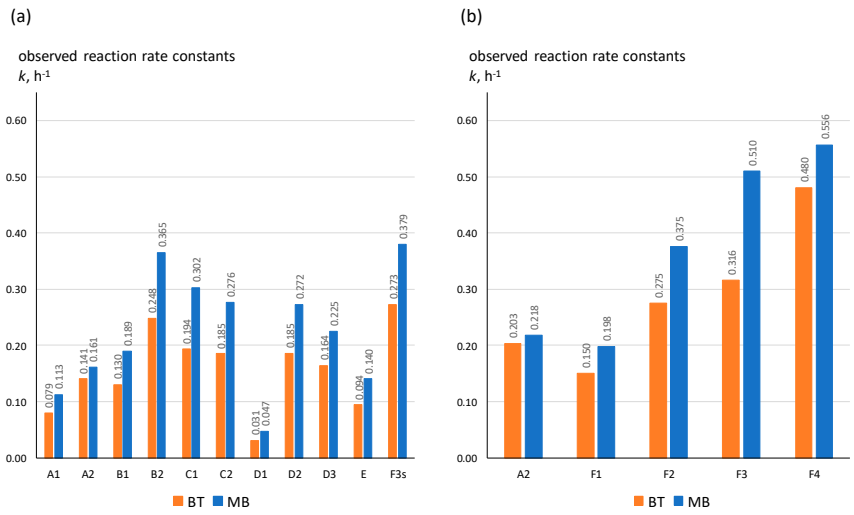

Figure 1. Comparison of the observed first-order reaction rate constants (k, min^{-1}) obtained for photocatalytic degradation of Methylene blue (MB) and 1H-benzotriazole (BT) in small photocatalytic cell reactor over a variety of photocatalysts (Table 1) with different film surface: (**a**) 0.5 cm^2 and (**b**) 2 cm^2.

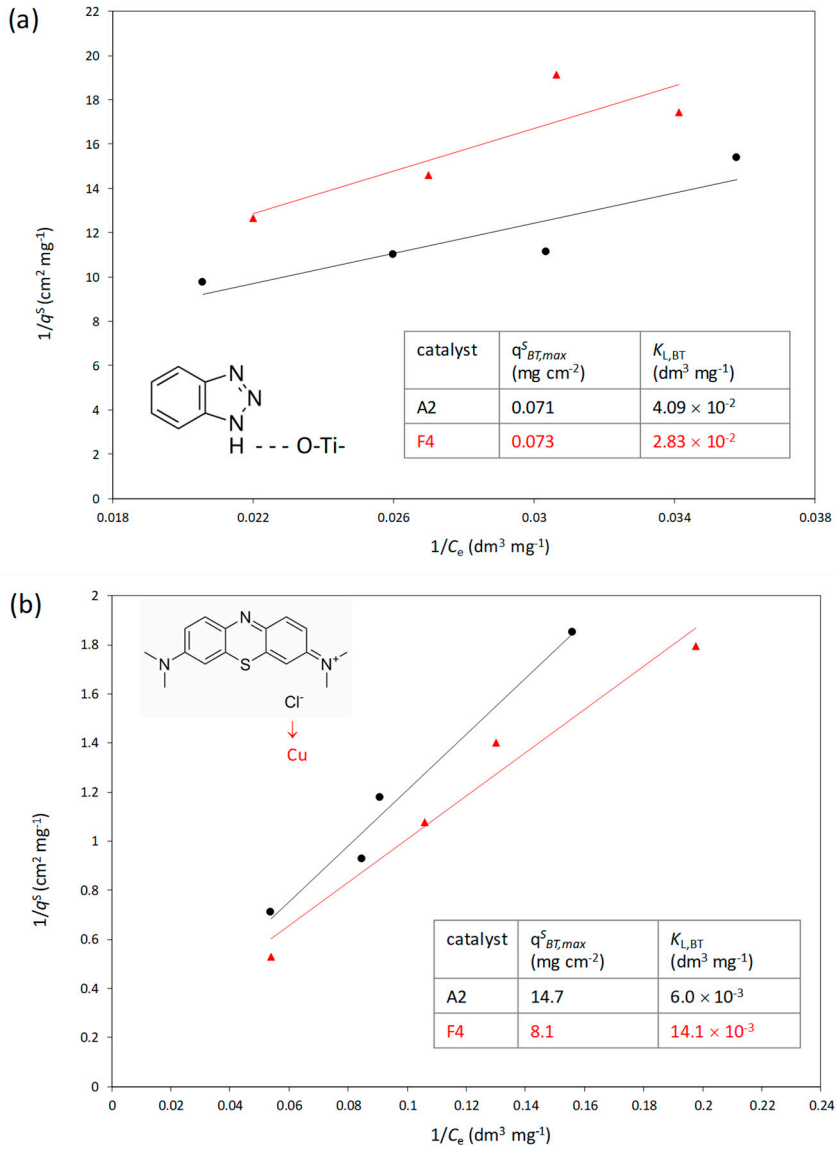

Figure 2. Langmuir isotherms for BT (**a**) and MB (**b**) adsorption on photocatalytic films A2 (R^2 values were 0.9140 and 0.9761, respectively) and F4 (R^2 values were 0.8522 and 0.9683, respectively); tentative binding and adsorption parameters are embedded in the graph (T = 23 ± 3 °C).

Table 1. Photocatalyst overview.

Mark	Full Sample Name	Preparation Method	Copper Source	k (BT)/h^{-1}	k (MB)/h^{-1}
A1	NEA TiO_2	Anodization	/	0.079	0.113
A2	NP TiO_2	Anodization and annealing	/	0.141	0.198
B1	HT_NP_TiO_2_oCu_0.025 M	Hydrothermal synthesis	$Cu(acac)_2$	0.130	0.161
B2	HT_NP_TiO_2_Cu_0.025 M	Hydrothermal synthesis	$Cu(NO_3)_2$	0.248	0.365
C1	ED_NP_TiO_2_oCu_0.05M_5 min	Electrodeposition	$Cu(acac)_2$	0.194	0.302
C2	ED_NP_TiO_2_Cu_0.05M_5 min	Electrodeposition	$Cu(NO_3)_2$	0.185	0.276
D1	NP_TiO_2_sCu_g_10V_20 min	Anodization with Cu source	$Cu(acac)_2$	0.031	0.047
D2	NP_TiO_2_sCu_g_20V_20 min	Anodization with Cu source	$Cu(NO_3)_2$	0.185	0.272
D3	NP_TiO_2_sCu_g_30V_20min	Anodization with Cu source	$Cu(NO_3)_2$	0.164	0.225
E	SC_NP_TiO_2_Cu_0.250 M	Spin coating	$Cu(NO_3)_2$	0.094	0.140
F1	0.0625 M	Spin coating	$Cu(acac)_2$	0.150	0.198
F2	0.125 M	Spin coating	$Cu(acac)_2$	0.275	0.375
F3s	0.250 M	Spin coating	$Cu(acac)_2$	0.273	0.379
F3	0.250 M	Spin coating	$Cu(acac)_2$	0.316	0.510
F4	0.500 M	Spin coating	$Cu(acac)_2$	0.480	0.556

Results are given for both referent photocatalysts and for the Cu-modified photocatalyst. In the case of BT, adsorption isotherms followed the same trend, and the obtained $q^S{}_{BT}$ and $K_{L,BT}$ are almost the same (values embedded in Figure 2). On the other hand, isotherm for MB adsorption on referent catalyst with nanoporous TiO_2 differed from the one obtained for the adsorption on Cu-modified catalyst. The surface coverage increased rapidly with the increase of the film surface and the concentration of dissolved MB. The explanation for the observed phenomenon can be described by the model pollutant structure. Namely, BT structure consists of a five-membered ring with three nitrogen atoms directly bonded to one another as substituents on a benzene ring (Figure 2). This compound presumably attaches to the film surface via hydrogen bond between H atom in the BT structure and O atom in the lattice, i.e., on the nanoporous TiO_2 surface. Cu had no significant effect on the binding of BT on the film. However, lower $q^S{}_{BT}$ and $K_{L,BT}$ in the case of Cu-modified catalysts, can be explained by the coverage of the surface by Cu-based compound, causing the decreased availability of O centers on the surface.

The MB molecule is different; MB is a thiazine dye with a dimethyl amide auxiliary group. MB exists as the chloride salt, and the presence of chlorine in the molecule can account for an additional binding via Cu on the surface.

Due to the difference in the adsorption mechanism, more detailed kinetics of photocatalytic degradation of BT and MB was studied using Langmuir–Hinshelwood model (Equations (3) and (4)).

$$r_i = \frac{d[\mathrm{BT}]}{dt} = \frac{k_{a,\,BT} K_{L,\,BT}}{1 + K_{L,\,BT}[\mathrm{BT}]_0}[\mathrm{BT}] \tag{3}$$

$$r_i = \frac{d[\mathrm{MB}]}{dt} = \frac{k_{\mathrm{a,\,MB}} K_{L,\,MB}}{1 + K_{L,\,MB}[\mathrm{MB}]_0}[\mathrm{MB}] \tag{4}$$

Note that the binding constant used in the kinetics model was the same as the one calculated from the adsorption isotherm, $K_{L,i}$. The k_a stands for the apparent reaction rate constant. This constant highly depends on the concentration of the pollutants on the surface and in the boundary layer, surface coverage (ϕ), catalysts optical properties such as specific absorption and scattering of the incident irradiation, and the intensity of the applied irradiation. The introduction of the term $q^S{}_i$ in Equation (2) allowed the interpretation of the results independent from the irradiated surface, i.e., it allowed a more in-depth analysis. The idea of surface-related amounts instead of the adsorbed amount per mass of catalyst proven beneficial for a surface phenomenon such as thin-layer photocatalysis since given constants in applied Langmuir-Hinshelwood (LH) model is more significant. Kinetic parameters form LH (Langmuir-Hinshelwood) models are summarized in Table 2.

Table 2. Kinetic parameters from the LH model (photocatalytic film surface 2 cm^2, otherwise stated).

Mark	Sample	Pollutant (*i*)	$k_{a,i}$, mg dm^{-3} min^{-1}	Average R^2
A2	NP TiO_2	BT	1.05 ± 0.02 (0.17 ± 0.00 *)	0.9805
		MB	0.60 ± 0.01	
		MB (low C_0)	5.00 ± 0.03	
F1	0.0625 M	BT	0.55 ± 0.00	0.9645
F2	0.125 M	BT	1.32 ± 0.02	0.9913
F3s	0.250 M	BT	0.35 ± 0.00	0.9543
F3	0.250 M	BT	1.45 ± 0.02	0.9778
F4	0.500 M	BT	1.70 ± 0.04 (0.36 ± 0.00 *)	0.9861
		MB	0.61 ± 0.01	
		MB (low C_0)	2.40 ± 0.01	

* for the film surface of 0.5 $cm^{2.}$

The determined apparent reaction rate constant revealed that the film F4 contained the optimal Cu loading for the enhancement of the activity under solar irradiation despite the lower binding of the

BT on the surface of the photocatalyst. The ratios of the $k_{a,i}$ determined for larger (2 cm^2), and small samples (0.5 cm^2), are around 4–5 for the films prepared in both sizes (A2 and F3/F3s). This revealed the effect of the surface coverage (ϕ) on the apparent rate constant. The surface ratio between samples was exactly four and the observed results indicate the uniform distribution of pollutants on the film surface, as the straightforward increase in apparent reaction rate constant, was expected.

As shown in Figure 3, BT photocatalytic degradation can be well described by the Langmuir-Hinshelwood model. However, degradation strongly depends on the film's surface area. Four times higher surface lead to a notably higher degree of degradation. Results for MB are somewhat different. The use of films with the larger surface will influence the initial adsorption equilibrium (achieved in the dark), but the higher degree of degradation was not observed during the photocatalytic process. The MB molecule binds to the film surface rapidly in the first 15 min forming a layer of adsorbed molecules that act as a filter for incident irradiation. The observed effect is more evident in the case of Cu-modified catalysts since the existence of chlorine in the dye structure leads to electrostatic interactions with Cu centers on the film surface. There are two different degradation pathways reported for MB [47]: first one related to the degradation of thiazine chromophore and the second dominated by the auxochome group degradation. In the current study, a slight shift in the absorption maximum for MB was observed by the end of experiments, which is a confirmation of the changes in the auxochrome. The additional set of experiments was done using the lower initial MB concentration. The obtained results confirmed the assumed filtering effect of the MB on the film surface. Namely, the apparent reaction rate constant is higher in the case of low initial MB concentrations (Table 2).

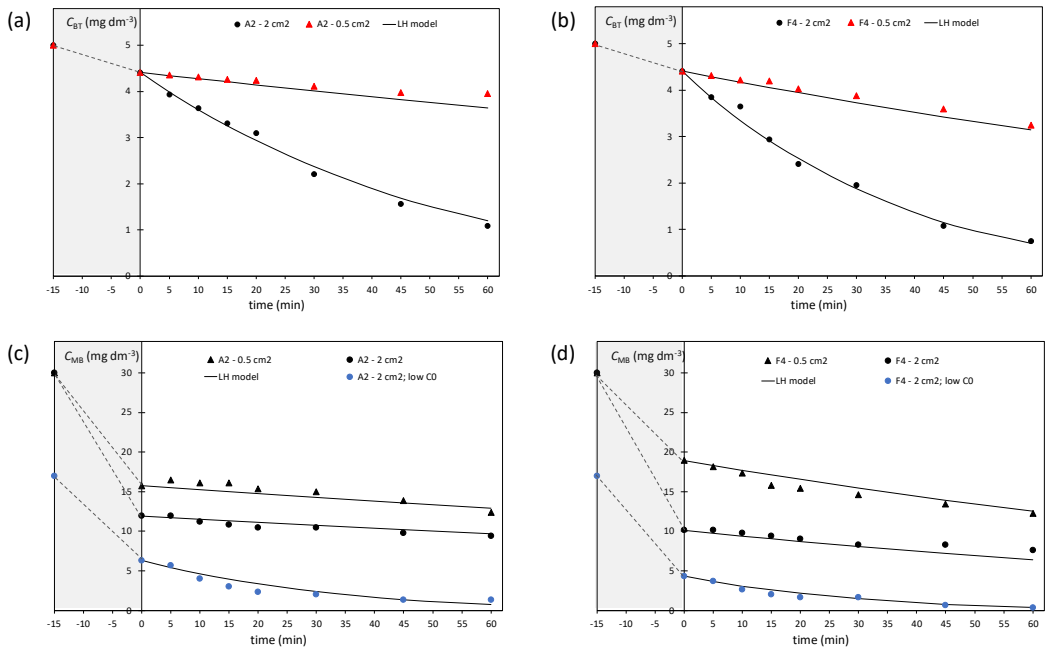

Figure 3. Kinetics of the photocatalytic degradation of BT (**a**,**b**) and MB (**c**,**d**) over irradiated films A2 and F4 in specially designed photoreactor. Grey areas denote the adsorption in the dark to achieve equilibrium.

MB was used as a reference, but this study showed that dye typically used in the photocatalytic test was not appropriate for the estimation of the photocatalytic activity of Cu-modified photocatalytic films. The primary goal was to check the possibility of fast degradation of BT by new catalysts under solar irradiation since BT is widely present in the environment. Photocatalytic films prepared by spin-coating (F1 to F4) showed acceptable activities. To check the film stability, each film was used in four consecutive cycles (Figure 4). The film was washed and air-dried between the cycles. Note that

each experiment in the cycle was done in triplicates, and the four cycles actually represent twelve 1-h experiments.

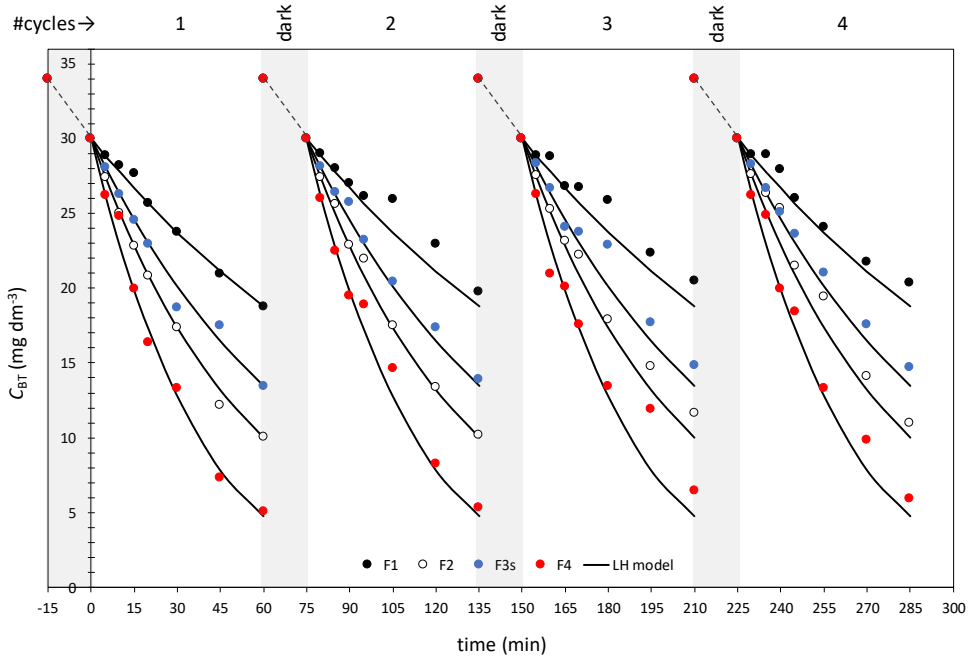

Figure 4. Kinetics of BT degradation over spin-coated films (F1, F2, F3, and F4) modified by Cu in four consecutive cycles.

Results from the cycles were compared to the values predicted by the LH model (Equation (3)). The good fit was obtained, proving the appropriate activity and the robustness of the new films.

Since the F series of samples, which were modified with Cu-based compounds using the spin-coating technique, showed the best photocatalytic performances among all studied samples, the morphology and the structure of this series (Table 2) were studied in details. Different analytical and spectroscopic techniques were used to determine morphology and crystal structures present in the unmodified and Cu-modified nanoporous TiO_2 photocatalyst were investigated by the Grazing incidence X-ray diffraction, structural phase of the samples was examined by confocal micro-Raman spectroscopy, and the morphology of the unmodified and Cu-modified NP TiO_2 samples was investigated by high resolution scanning electron microscope with field emission gun cathode (FEG-SEM).

2.2. Structural Properties

2.2.1. Grazing Incidence X-ray Diffraction (GIXRD) Results

GIXRD diffractograms of unmodified nanoporous TiO_2 and Cu-modified thin films are shown in Figure 5 along with calculated diffractions for anatase TiO_2, hexagonal α-Ti (substrate) and measured organometallic copper compounds ($Cu(acac)_2$ + 2-propoxyethanol) which were used as reference profiles. As can be seen, GIXRD discloses anatase TiO_2 as the dominant phase present in all films. Cu-modified samples with a lower concentration of Cu-based compounds (0.0625 M and 0.125 M) have diffraction patterns similar to unmodified nanoporous TiO_2, showing only peaks that can be attributed to TiO_2. For the samples with a higher Cu concentration (0.250 M and 0.500 M), peaks that appear at 2θ around 24.7°, 26.1°, 27.3°, 30.4°, and 31.5°, can be attributed to an organometallic copper compound ($Cu(acac)_2$ + 2-propoxyethanol). This result indicates that the drying of the modified samples for 1 h at 150 °C did not induce degradation of the used Cu-based compounds.

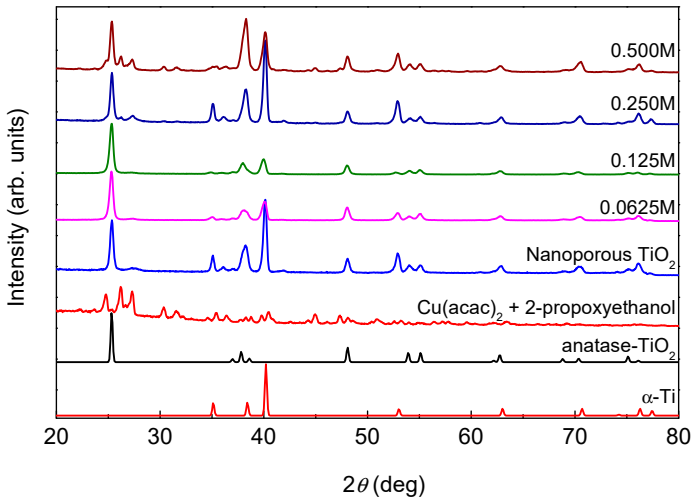

Figure 5. GIXRD diffractograms of nanoporous TiO_2 and Cu-modified immobilized nanoporous TiO_2 samples with different concentrations of Cu-based compounds. α-Ti Bragg peaks originate from the substrate. The diffractograms are normalized with respect to the (101) anatase Bragg reflection at $2\theta = 25.33°$.

2.2.2. Raman Spectroscopy Results

The confocal micro-Raman spectra of all samples contained five characteristic bands that are assigned to anatase TiO_2 crystalline phase (144, 199, 396, 514, and 636 cm^{-1}) [48]. In Figure 6, only a representative spectrum of the Cu-modified sample is shown (0.250 M), since the same results were obtained for all Cu-modified samples. This result indicates that by annealing of the nanoporous TiO_2 at 450 °C, only the anatase form of TiO_2 is obtained, which is in agreement with GIXRD results. The spectra recorded on micro-crystals present on the surface of the samples prepared with higher concentrations of Cu-based compounds (0.250 M and 0.500 M), showed additional Raman bands at 203 cm^{-1} and 448 cm^{-1}. These bands can be attributed to $Cu(acac)_2$ by comparison with the Raman spectra of the precursor ($Cu(acac)_2$ in 2-propoxyethanol).

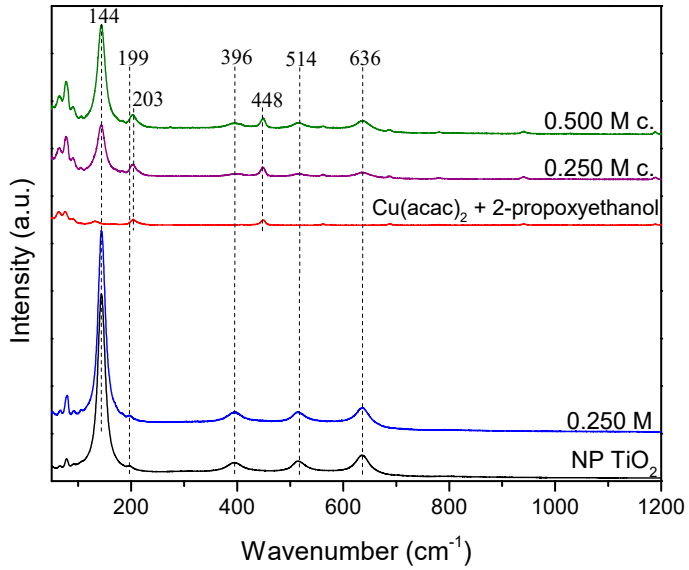

Figure 6. Micro-Raman spectra of nanoporous (NP) TiO_2 and Cu-modified NP TiO_2. The position of the Raman active TiO_2 bands, as well as bands of organometallic Cu compounds ($Cu(acac)_2$ + 2-propoxyethanol), are shown above spectra. The spectra denoted by c. are recorded at micro-crystals observed on the surface of the samples.

2.2.3. High-Resolution Scanning Electron Microscopy Results

We investigated the morphology of the unmodified and Cu-modified NP TiO_2 samples by a high-resolution scanning electron microscope with field emission gun cathode (FEG-SEM). With the aim to conclude the formation of Cu-based compounds on the surface of NP TiO_2, top-view FEG-SEM images were recorded (Figure 7a). Nanoporous TiO_2 obtained by a simple anodization process shows homogenous pores that occasionally form uniform nanotube arrays with slightly varying length (Figure 7a, NP TiO_2). The inner diameters of the nanopores were in the range of 90–100 nm and outer diameters in the range of 110–120 nm. The Cu-modified samples (0.0625 M, 0.125 M, 0.250 M, and 0.500 M) do not show significant changes in the morphology of NP TiO_2 (Figure 7a), except for the presence of few nanoparticles or nano-agglomerates on the surface of the pores. The amount of the nano-structures formed on the surface of the pores slightly varies, indicating the formation of different quantity of Cu-based nanostructures. To determine elemental composition of the Cu-modified nanoporous TiO_2, energy dispersive X-ray spectroscopy (EDS) was used (Figure 7b). EDS spectra of Cu-modified samples show Cu besides Ti and O. Three peaks observed at 0.39, 4.5, and 4.9 keV in the EDS spectra correspond to titanium and peak at 0.5 keV corresponds to oxygen. Furthermore, copper peaks are clearly visible at 0.9 and 8.0 keV (Figure 7b).

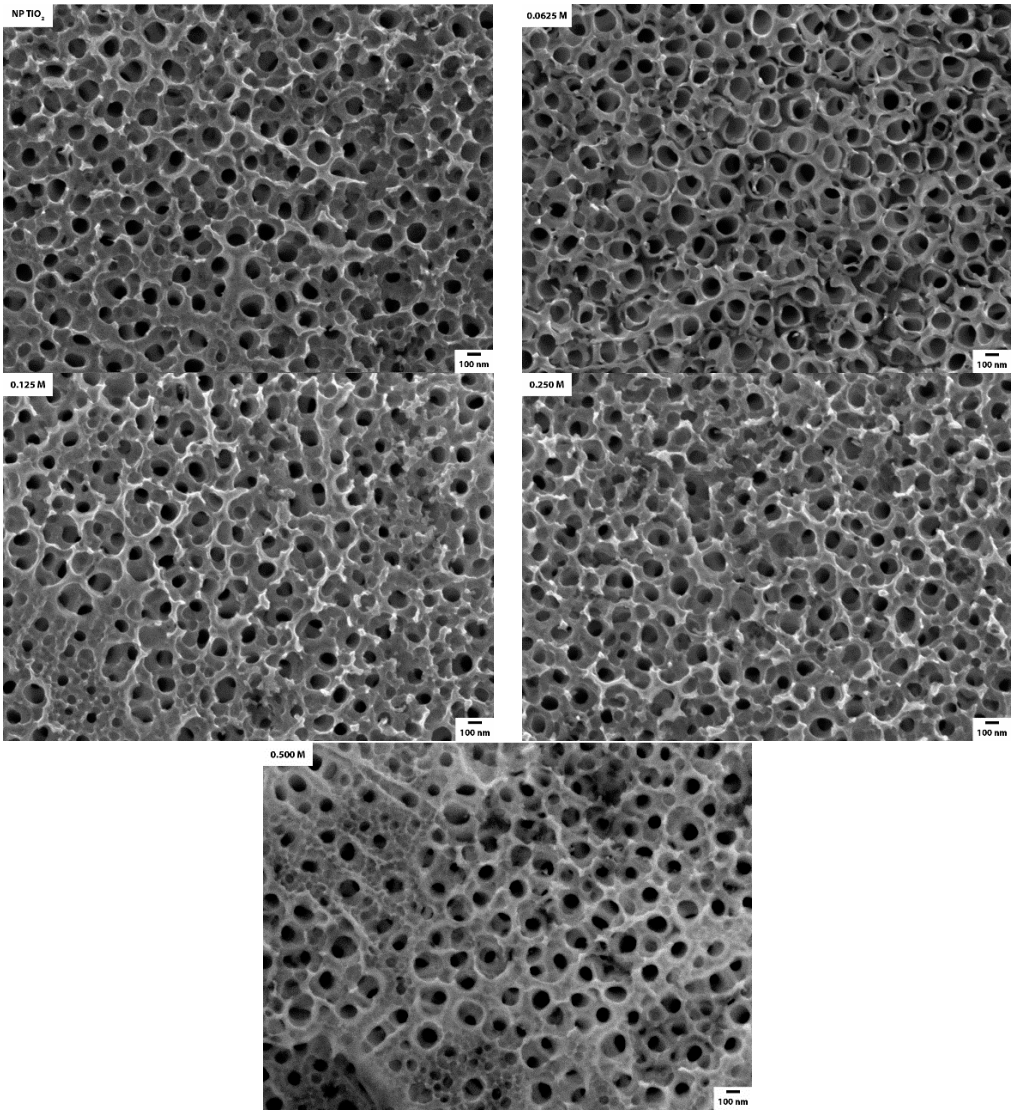

(a)

Figure 7. *Cont.*

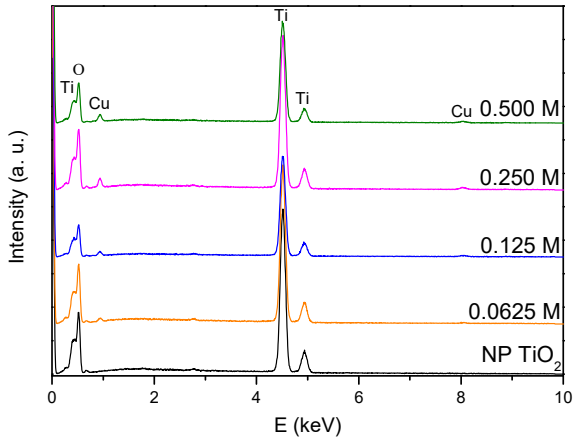

(**b**)

Figure 7. (**a**) Micrographs of the unmodified and Cu-modified NP TiO_2 with various Cu concentrations (from 0.0625 to 0.500 M) and (**b**) qualitative EDS spectra of the given samples.

In Figure 8, examples of the surfaces on which EDS (Energy Dispersive X-ray Spectroscopy) spectra were recorded are shown for two Cu-modified samples (0.125 M and 0.500 M).

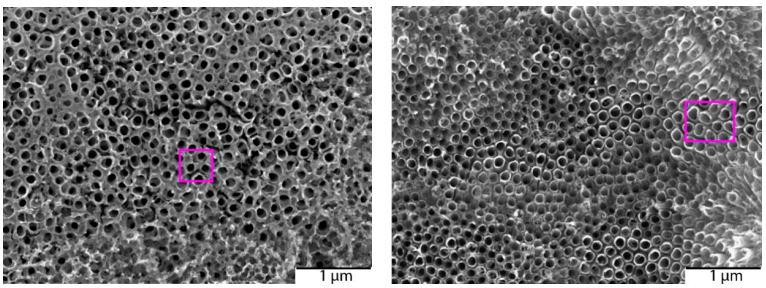

(**a**) (**b**)

Figure 8. The rectangular magenta line on the sample is the area analyzed by the EDS for: (**a**) Cu-modified nanoporous TiO_2 with 0.125 M and (**b**) with 0.500 M Cu-based compounds.

The EDS results obtained on the surface of all NP TiO_2 (without micro-crystals) are shown in Table 3. Results confirmed that surface modification with copper was successful (0.76 to 2.25 at.% of Cu). It was observed that the atomic percentage of Cu increased in the samples with a higher concentration of Cu-based compounds, but the amount of Cu did not increase proportionally with the starting Cu concentration.

Table 3. Results of EDS measurements.

Sample	Ti K (at.%)	O K (at.%)	Cu K (at.%)
NP TiO_2	32.53	67.47	0
0.0625 M	32.26	66.98	0.76
0.125 M	35.45	62.96	1.59
0.250 M	31.36	66.61	2.03
0.500 M	31.83	65.92	2.25

Raman bands of the Cu-based compounds ($Cu(acac)_2$ in 2-propoxyethanol) were observed only on the micro-crystal residues on the surface of the Cu-modified samples (Figure 6), while the presence of Cu was also observed on the surface of Cu-modified nanoporous TiO_2 without crystals. That finding indicates the possibility of the formation of pure Cu or Cu-based oxide nano-agglomerates/nanostructures on the surface of the samples (Figure 7a). These results indicate

that residual $Cu(acac)_2$ complex crystals are expected at higher Cu concentrations. It is in agreement with micro-Raman spectra and also confirmed by FEG-SEM and EDS (Figure 9). The EDS spectrum of the micro-crystal (Figure 9) showed 9.13 at.% of Cu and 46.04 at.% of C. This additionally confirms that micro-crystals have a composition of the residual $Cu(acac)_2$ complex.

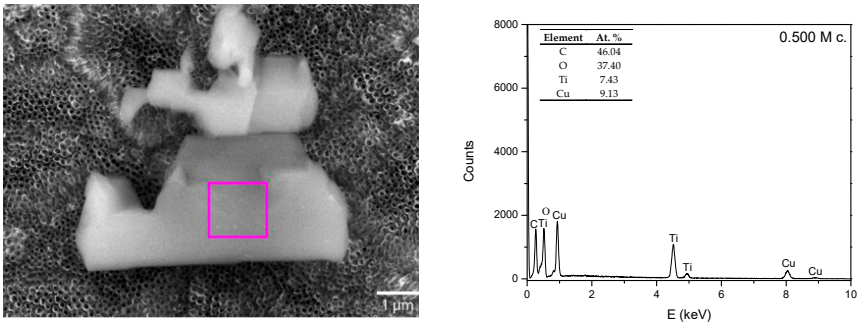

Figure 9. FEG-SEM micrograph of the Cu-modified NP TiO_2 and qualitative EDS spectra of 0.500 M acquired on the microcrystal.

3. Materials and Methods

3.1. Catalyst Preparation

The following materials were used: titanium foil (2 × 2 cm, thickness 0.25 mm, 99.7%, Sigma-Aldrich, Co., 3050 Spruce Street, St.Louis, MO, USA), ethanol (C_2H_5OH, 99.8%, Riedel-de Haen, 1953S.Harvey St., Muskegon, MI, USA), deionized water, ammonium fluoride (NH_4F, 99.9%, Sigma-Aldrich CHEMIE GmbH, Riedstr. 2, D-89555 Steinheim 49), ethylene glycol ($C_2H_6O_2$, 99.5%, Riedel-de Haen, 1953S.Harvey St., Muskegon, MI, USA), cooper (II) nitrate trihydrate ($(Cu(NO_3)_2{\cdot}3H_2O$, 99%, Carlo Erba Reagents S.A.S., BP 616, F-27016 Val de Reuil Cedex), copper (II) acetylacetonate ($(Cu(C_5H_7O_2)_2$, 98%, Acros Organics, NJ, USA), 2-propoxyethanol ($C_5H_{12}O_2$, 98%, Acros Organics, NJ, USA). All of the chemicals were used without further purification.

Nanoporous TiO_2 samples were obtained by anodizing titanium metal foil. Anodization was carried out at the room temperature using a direct current (DC) power supply in a conventional two-electrode cell. Ti-foil was used as the anode, and Pt foil served as the counter electrode. Ethylene glycol containing 0.3 wt.% NH_4F and 12 vol.% distilled water was used as an electrolyte. Nanoporous amorphous TiO_2 samples (denoted as NEA TiO_2 (not-annealed TiO_2) in Table 1) that also contained a small amount of self-organized and aligned TiO_2 nanotubes/nanopores, were fabricated at 60 V for 3 h. After anodization, samples were rinsed first in ethanol then in deionized water, and dried using nitrogen gas. Finally, anodized samples were thermally treated in a tube furnace at 450 °C (heating/cooling rate of 2 °C/min) for 2 h to obtain pure anatase form of TiO_2 [29,49] (denoted as NP TiO_2 in Table 1). A modified version of anodization process was also carried out with addition of copper nitrate (samples NP_TiO_2_sCu_g_20V_20min and NP_TiO_2_sCu_g_30V_20min, Table 1) or copper acetylacetonate (sample NP_TiO_2_sCu_g_10V_20min, Table 1) in electrolyte as one of the syntheses method.

Furthermore, Cu-modified nanoporous TiO_2 samples were prepared by an additional three different synthesis methods: hydrothermal synthesis, electrodeposition, and spin-coating. The hydrothermal synthesis was carried out in a Teflon autoclave reactor at 150 °C for 6 h. As-prepared nanoporous TiO_2 samples were put inside autoclave reactor together with a 25 mM of an aqueous solution of copper nitrate (sample HT_NP_TiO_2_Cu_0.025M, Table 1) or copper acetylacetonate (sample HT_NP_TiO_2_oCu_0.025M, Table 1). After synthesis, samples were carefully rinsed several times with distilled water to remove organic residuals.

For electrodeposition, the two-electrode system was used. Modification was done with 0.05 M solution of copper nitrate (sample ED_NP_TiO_2_Cu_0.05M_5min, Table 1) or copper acetylacetonate

(sample ED_NP_TiO_2_oCu_0.05M_5min, Table 1) electrolyte using nanoporous TiO_2 as cathode and platinum as anode. The copper modification was done by applying 4 V voltage between anode and cathode. Five minutes was required to achieve Cu-modified nanoporous TiO_2. As-fabricated Cu-modified samples were thermally annealed to obtain crystalline Cu-modified TO_2 nanostructures.

Nanoporous TiO_2 samples were used as the substrates for thin films prepared by spin-coating. The films were formed from the 100 µL of coating solution: copper nitrate in ethanol (sample SC_NP_TiO_2_Cu_0.250M, Table 1) or, alternatively, copper acetylacetonate in 2-propoxyethanol (0.0625 M, 0.125 M, 0.250 M, and 0.500 M). Samples were denoted F1, F2, F3, and F4, respectively (Table 1). Solutions were deposited on the surface of the samples by spin-coating in an ambient atmosphere at a speed of 2000 rpm for 30 s. Cu-modified samples were dried on a hotplate at 150 °C for 1 h. Since the F series was additionally tested, all spin-coated samples (F1, F2, F3 and F4) and reference sample A2 were synthesized in triplicates.

3.2. Catalyst Characterization

3.2.1. Photocatalytic Activity Tests

3.2.1.1. Photoreactor Setup

Experiments were performed in the specially designed photoreactor known as the small photocatalytic cell (hereafter: SPC). The SPC setup consisted of the irradiation source, flow cell in the form of a shallow open cylinder, and a pump (Figure 10). In a typical experiment, the photocatalytic film is placed on the bottom of the cell, and the model solution runs through the cell in total recirculation (Q = 120 mL min^{-1}). The photocatalytic film is directly irradiated from above, so the catalysts were positioned perpendicular to the light irradiation. Prior to experiments, 1H-benzotriazole (BT) ($C_6H_5N_3$, 99%, Acros Organics, NJ, USA), or methylene blue (MB) ($C_{16}H_{18}ClN_3S$, p.a. Kemika, Zagreb, Croatia) solutions (C_0 = 30 mg dm^{-3}; otherwise stated) were recirculated in the dark over the plates to achieve the sorption equilibrium. The source of irradiation was full-spectrum compact fluorescent bulb simulating solar spectra with high UVB (Ultraviolet rays); high color rendering Ra98/Class 1A with color temperature of 6500 K (JBL Reptil Desert UV, 15W). The lamp was placed in the special conical housing with the reflective inner surface. Such setup ensures the isoactinic conditions in the flow cell. The ultraviolet (UV) rays; UVB and UVA (Ultraviolet rays) intensities were measured by UVP UVX radiometer, fitted with the corresponding UVB and UVA sensors, matching the distance of the photocatalytic film surface. Intensities at film surface, which were accounted for the incident photon flux at photocatalysts surface, were: I_{UVB} = 0.18 $mWcm^{-2}$ and I_{UVA} = 2.45 $mWcm^{-2}$. Experiments were performed in quadruplicates to discard possible experimental error and to check the reusability and the stability of the photocatalysts. Control experiments were performed without the catalysts to study the photolysis of the model pollutants.

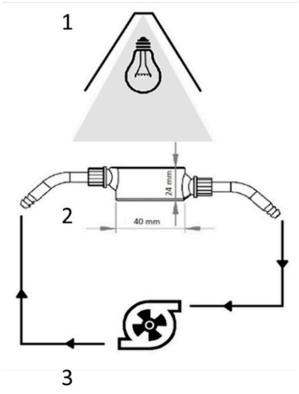

Figure 10. Schematics of the SPC: 1—irradiation source, 2—flow cell (V = 30 mL), and 3—peristaltic pump with hosing (V_{total} = 100 mL).

3.2.1.2. Analyses

The degradation of BT and MB in the samples was evaluated in terms of respective concentrations decrease. The concentration of BT was determined using HPLC, Knauer, with SUPELCO C18 column, length 250 mm, internal diameter 4.6 mm, and UV detection at 275 nm. The analyses were carried out using isocratic mode with the mobile phase consisted of methanol and water (1:1) at a flow rate of 1.0 mL min^{-1}.

The MB concentration was determined using the spectrophotometric analysis at λ = 660 nm, using a modular spectrophotometer Ocean Optics USB2000+ with deuterium and halogen emission source and quartz cuvette (1 × 1 cm). The concentration was calculated using the Lambert-Beer equation whereby the light path was 1 cm, and the extinction coefficient was $\varepsilon_{MB} = 2.964 \times 10^{-2}$ dm^3 mg^{-1} cm^{-1}.

3.2.2. Grazing Incidence X-ray Diffraction (GIXRD) Analysis

The crystalline structure of the unmodified and Cu-modified nanoporous TiO_2 was investigated using Siemens D5000 diffractometer in parallel beam geometry with Cu K-α radiation, a point detector and a collimator in front of the detector. Grazing incidence X-ray diffraction (GIXRD) scans were performed with the constant incidence angle $\alpha_i = 1°$, guaranteeing that the information contained in the scattered signal covers the entire film volume, i.e., ensuring a maximum diffraction yield from thin films.

3.2.3. Raman Spectroscopy

The structural phase of unmodified and Cu-modified nanoporous TiO_2 was studied by confocal micro-Raman spectroscopy, using Jobin Yvon T64000 (Japan) with a solid-state laser operated at 532.5 nm for excitation. The objective with 50× magnification (Olympus, Tokyo, Japan) and large working distance was used. The power of the laser was 25 mW. It was optimized to avoid heating in the focus of the laser beam that could induce the phase transition of TiO_2.

3.2.4. Scanning Electron Microscopy (SEM) and Energy-Dispersive X-ray Spectroscopy (EDS)

Morphology and elemental composition of the surface were investigated using field emission gun scanning electron microscopy (FEG-SEM) device JEOL model 7000F operating at 15 kV equipped with energy dispersive X-ray analyzer (Oxford Instruments EDS/INCA 350, Japan) attached to the above-described microscope. Spectra were recorded at 15 kV accelerating voltage and 10 mm working distance.

4. Conclusions

In this research, we have modified nanoporous TiO_2 photocatalysts with Cu-based compounds. Four different synthesis methods were used for Cu-based modification of nanoporous TiO_2: hydrothermal synthesis, anodization with Cu source, electrodeposition and spin-coating. The focus was put on Cu-modified nanoporous TiO_2 samples synthesized by spin-coating technique, modified with four different concentrations of Cu-based compounds (0.0625, 0.125, 0.25, and 0.5 M). Those samples showed the highest photocatalytic activity under UV/Vis irradiation. This result confirmed the importance of preparation method and the concentration of Cu-based compounds deposited on the surface of the nanoporous TiO_2 on the observed photocatalytic activity.

Samples synthesized with spin-coating and hydrothermal synthesis have similar photocatalytic activity, but spin-coating is the simplest method and therefore studied in detail. Photocatalytic activity measurements for the most active among samples prepared by spin-coating (F4) showed a 2.8 times increase in the MB degradation and 3.4 in BT degradation in comparison to the unmodified nanoporous TiO_2 sample (A2) that have similar behavior as commercial TiO_2 P25 [29]. Furthermore, we confirmed that the film surface has a large influence on the photocatalytic activity, i.e., four times larger surface lead to the 5 to 6 times increase in the photocatalytic activity.

Photocatalytic thin films are stable, completely attached to the nanoporous TiO_2 plates, and after the photocatalytic reaction, plates can be easily removed from the solution. Since spin-coating is a low-cost, fast, and most common technique for applying thin films on the substrates, these photocatalysts could be used on a larger scale.

Author Contributions: Conceptualization—T.Č. and I.P.; validation—A.G., T.Č.; investigation—K.S., L.R., J.M., I.G., I.P., A.G.; resources—A.G.; data curation—T.Č. and I.G.; writing—original draft preparation—T.Č., I.G. and A.G.; writing—review and editing—A.G.; visualization—T.Č.; supervision—A.G.; funding acquisition—A.G. All authors have read and agreed to the published version of the manuscript.

Funding: This work was supported by the Ministry of science and education of Croatia under the project HrZZ-IP-2018-01-5246, Centre of Excellence for Advanced Materials and Sensing Devices, Ruđer Bošković Institute, Zagreb, Croatia, KK.01.1.1.01.0001 and partially supported by European Regional Development Fund (ERDF) under the (IRI) project "Improvement of solar cells and modules through research and development" (KK.01.2.1.01.0115).

Conflicts of Interest: The authors declare no conflict of interest. The funders had no role in the design of the study; in the collection, analyses, or interpretation of data; in the writing of the manuscript, or in the decision to publish the results.

References

1. Fujishima, A.; Rao, T.N.; Tryk, D.A. Titanium dioxide photocatalysis. *J. Photochem. Photobiol. C* **2000**, *1*, 1–21. [CrossRef]
2. Zou, Z.G.; Ye, J.H.; Sayama, K.; Arakawa, H. Direct splitting of water under visible light irradiation with an oxide semiconductor photocatalyst. *Nature* **2001**, *414*, 625–627. [CrossRef] [PubMed]
3. Asahi, R.; Morikawa, T.; Ohwaki, T.; Aoki, K.; Taga, Y. Visible-light photocatalysis in nitrogen-doped titanium oxides. *Science* **2001**, *293*, 269–271. [CrossRef] [PubMed]
4. Malato, S.; Caceres, J.; Aguera, A.; Mezcua, M.; Hernando, D.; Vial, J.; Fernandez-Alba, A.R. Degradation of Imidacloprid in Water by Photo-Fenton and TiO_2 Photocatalysis at a Solar Pilot Plant: A Comparative Study. *Environ. Sci. Technol.* **2001**, *35*, 4359–4366. [CrossRef] [PubMed]
5. Nagaveni, K.; Sivalingam, G.; Hegde, M.S.; Madras, G. Photocatalytic Degradation of Organic Compounds over Combustion-Synthesized Nano-TiO_2. *Environ. Sci. Technol.* **2004**, *38*, 1600–1604. [CrossRef]
6. Petronellaa, F.; Truppia, A.; Ingrossoa, C.; Placidoa, T.; Striccolia, M.; Curria, M.L. Nanocomposite materials for photocatalytic degradation of pollutants. *Catal. Today* **2017**, *281*, 85–100. [CrossRef]
7. Guan, K. Relationship between photocatalytic activity, hydrophilicity and self-cleaning effect of TiO_2/SiO_2 films. *Surf. Coat. Technol.* **2005**, *191*, 155–160. [CrossRef]
8. Hoffmann, M.R.; Martin, S.T.; Choi, W.; Bahnemann, D.W. Environmental Applications of Semiconductor Photocatalysis. *Chem. Rev.* **1995**, *95*, 69–96. [CrossRef]
9. Matthews, R.W. Photooxidation of organic impurities in water using thin films of titanium dioxide. *J. Phys. Chem.* **1987**, *91*, 3328–3333. [CrossRef]
10. Zhang, L.; Dillert, R.; Bahnemann, D.; Vormoor, M. Photo-induced hydrophilicity and self-cleaning: Models and reality. *Environ. Sci.* **2012**, *5*, 7491–7507. [CrossRef]
11. Grätzel, M. Recent advances in sensitized mesoscopic solar cells. *Acc. Chem. Res.* **2009**, *42*, 1788–1798. [CrossRef] [PubMed]
12. Manassero, A.; Satuf, M.L.; Alfano, O.M. Photocatalytic reactors with suspended and immobilized TiO_2: Comparative efficiency evaluation. *Chem. Eng. J.* **2017**, *326*, 29–36. [CrossRef]
13. Roy, P.; Berger, S.; Schmuki, P. TiO_2 nanotubes: Synthesis and applications. *Angew. Chem. Int. Ed.* **2011**, *50*, 2904–2939. [CrossRef] [PubMed]
14. Yu, D.; Zhu, X.; Zhen, X.; Zhong, X.; Gui, Q.; Ye, S.; Zhang, S.; Chen, X.; Li, D. Facile method to enhance the adhesion of TiO_2 nanotube arrays to Ti substrate. *ACS Appl. Mater. Interfaces* **2014**, *6*, 8001–8005. [CrossRef] [PubMed]
15. Lee, K.; Mazare, A.; Schmuki, P. One-dimensional titanium dioxide nano-materials: Nanotubes. *Chem. Rev.* **2014**, *114*, 9385–9454. [CrossRef]
16. Paramasivam, I.; Macak, J.M.; Ghicov, A.; Schmuki, P. Enhanced photochromism of Ag loaded self-organized TiO_2 nanotube layers. *Chem. Phys. Lett.* **2007**, *445*, 233–237. [CrossRef]

17. Yang, K.; Dai, Y.; Huang, B.J. Understanding photocatalytic activity of S-and P-doped TiO_2 under visible light from first-principles. *Phys. Chem. C* **2007**, *111*, 18985–18994. [CrossRef]
18. Choi, W.; Termin, A.; Hoffmann, M.R. The Role of Metal Ion Dopants in Quantum-Sized TiO_2: Correlation between Photoreactivity and Charge Carrier Recombination Dynamics. *J. Phys. Chem.* **1994**, *98*, 13669–13679. [CrossRef]
19. Irie, H.; Kamiya, K.; Shibanuma, T.; Miura, S.; Tryk, D.A.; Yokoyama, T.; Hashimoto, K. Visible Light-Sensitive Cu(II)-Grafted TiO_2 Photocatalysts: Activities and X-ray Absorption Fine Structure Analyses. *J. Phys. Chem. C* **2009**, *113*, 10761–10766. [CrossRef]
20. Xin, B.; Jing, L.; Ren, Z.; Wang, B.; Fu, H. Effects of simultaneously doped and deposited Ag on the photocatalytic activity and surface states of TiO_2. *J. Phys. Chem. B* **2005**, *109*, 2805–2809. [CrossRef]
21. Wang, Z.; Lang, X. Visible light photocatalysis of dye-sensitized TiO_2: The selective aerobic oxidation of amines to imines. *Appl. Catal. B* **2018**, *224*, 404–409. [CrossRef]
22. Bahadur Rawal, S.; Bera, S.; Lee, D.; Jang, D.; Lee, W. Design of visible-light photocatalysts by coupling of narrow bandgap semiconductors and TiO_2: Effect of their relative energy band positions on the photocatalytic efficiency. *Catal. Sci. Technol.* **2013**, *3*, 1822–1830. [CrossRef]
23. Marschall, R.; Wang, L. Non-metal doping of transition metal oxides for visible-light photocatalysis. *Catal. Today* **2014**, *225*, 111–135. [CrossRef]
24. Sclafani, A.; Herrmann, J.M. Influence of metallic silver and of platinum-silver bimetallic deposits on the photocatalytic activity of titania (anatase and rutile) in organic and aqueous media. *J. Photochem. Photobiol. A* **1998**, *113*, 181–188. [CrossRef]
25. Klosek, S.; Raftery, D. Visible Light Driven V-Doped TiO_2 Photocatalyst and Its Photooxidation of Ethanol. *J. Phys. Chem. B* **2001**, *105*, 2815–2819. [CrossRef]
26. Macak, J.M.; Barczuk, P.J.; Tsuchiya, H.; Nowakowska, M.Z.; Ghicov, A.; Chojak, M.; Bauer, S.; Virtanen, S.; Kulesza, P.J.; Schmuki, P. Self-organized nanotubular TiO_2 matrix as support for dispersed Pt/Ru nanoparticles: Enhancement of the electrocatalytic oxidation of methanol. *Electrochem. Commun.* **2005**, *7*, 1417–1422. [CrossRef]
27. Haick, H.; Paz, Y. Long-Range Effects of Noble Metals on the Photocatalytic Properties of Titanium Dioxide. *J. Phys. Chem. B* **2003**, *107*, 2319–2326. [CrossRef]
28. Nguyen, N.T.; Ozkan, S.; Tomanec, O.; Zhou, X.; Zboril, R.; Schmuki, P. Nanoporous AuPt and AuPtAg alloy co-catalysts formed by dewetting-dealloying on ordered TiO_2 nanotube surface lead to significantly enhanced photocatalytic H_2 generation. *J. Mater. Chem. A* **2018**, *6*, 13599–13606. [CrossRef]
29. Plodinec, M.; Grčić, I.; Willinger, M.G.; Hammud, A.; Huang, X.; Panžić, I.; Gajović, A. Black TiO_2 nanotube arrays decorated with Ag nanoparticles for enhanced visible-light photocatalytic oxidation of salicylic acid. *J. Alloys Compd.* **2019**, *776*, 883–896. [CrossRef]
30. Chand, R.; Obuchi, E.; Katoh, K.; Luitel, H.N.; Nakano, K. Enhanced photocatalytic activity of TiO_2/SiO_2 by the influence of Cu-doping under reducing calcination atmosphere. *Catal. Commun.* **2011**, *13*, 49–53. [CrossRef]
31. Momeni, M.M.; Ghayeb, Y.; Ezati, F. Fabrication, characterization and photoelectrochemical activity of tungsten-copper co-sensitized TiO_2 nanotube composite photoanodes. *J. Colloid Interface Sci.* **2018**, *514*, 70–82. [CrossRef] [PubMed]
32. Janczarek, M.; Kowalska, E. On the Origin of Enhanced Photocatalytic Activity of Copper-Modified Titania in the Oxidative Reaction Systems. *Catalysts* **2017**, *7*, 317. [CrossRef]
33. Chan, G.H.; Zhao, J.; Hicks, E.M.; Schatz, G.C.; Van Duyne, R.P. Plasmonic properties of copper nanoparticles fabricated by nanosphere lithography. *Nano Lett.* **2007**, *7*, 1947–1952. [CrossRef]
34. Kowalska, E.; Prieto Mahaney, O.O.; Abe, R.; Ohtani, B. Visible-light-induced photocatalysis through surface plasmon excitation of gold on titania surfaces. *Phys. Chem. Chem. Phys.* **2010**, *12*, 2344–2355. [CrossRef] [PubMed]
35. Zhang, S.; Peng, B.; Yang, S.; Wang, H.; Yu, H.; Fang, Y.; Peng, F. Non-noble metal copper nanoparticles-decorated TiO_2 nanotube arrays with plasmon-enhanced photocatalytic hydrogen evolution under visible light. *Int. J. Hydrogen Energy* **2015**, *40*, 303–310. [CrossRef]
36. DeSario, P.A.; Pietron, J.J.; Brintlinger, T.H.; McEntee, M.; Parker, J.F.; Baturina, O.; Stroud, R.M.; Rolison, D.R. Oxidation-stable plasmonic copper nanoparticles in photocatalytic TiO_2 nanoarchitectures. *Nanoscale* **2017**, *9*, 11720–11729. [CrossRef] [PubMed]

37. Hussein, M.; Assadi, N.; Hanaor, D.A.H. The effects of copper doping on photocatalytic activity at (101) planes of anatase TiO_2: A theoretical study. *Appl. Surf. Sci.* **2016**, *387*, 682–689.
38. Li, J.; Zhen, D.; Sui, G.; Zhang, C.; Deng, Q.; Jia, L. Nanocomposite of Cu–TiO_2-SiO_2 with High Photoactive Performance for Degradation of Rhodamine B Dye in Aqueous Wastewater. *J. Nanosci. Nanotechnol.* **2012**, *12*, 6265–6270. [CrossRef]
39. Ohko, Y.; Noguchi, H.; Nakamura, Y.; Negishi, N.; Takeuchi, K. Highly Selective Photocatalytic Reduction of NO_2 in Air to NO Using Cu^{2+}-Loaded TiO_2 Thin Films. *J. Photochem. Photobiol. A* **2009**, *206*, 27–31. [CrossRef]
40. Miyauchi, M.; Irie, H.; Liu, M.; Qiu, X.; Yu, H.; Sunada, K.; Hashimoto, K. Visible-Light-Sensitive Photocatalysts: Nanocluster-Grafted Titanium Dioxide for Indoor Environmental Remediation. *J. Phys. Chem. Lett.* **2016**, *7*, 75–84. [CrossRef]
41. Yu, J.; Hai, Y.; Jaroniec, M. Photocatalytic Hydrogen Production over CuO-Modified Titania. *J. Colloid Interface Sci.* **2011**, *357*, 223–228. [CrossRef] [PubMed]
42. Jin, Q.; Fujishima, M.; Iwaszuk, A.; Nolan, M.; Tada, H. Loading Effect in Copper(II) Oxide Cluster-Surface-Modified Titanium(IV) Oxide on Visible-and UV-Light Activities. *J. Phys. Chem. C* **2013**, *117*, 23848–23857. [CrossRef]
43. Etape, E.P.; Ngolui, L.J.; Foba-tendo, J.; Yufanyi, D.M.; Namondo, B.V. Synthesis and Characterization of CuO, TiO_2, and CuO-TiO_2 Mixed Oxide by a Modified Oxalate Route. *J. Appl. Chem.* **2017**, *2017*, 1548654.
44. Wu, X.; Chou, N.; Lupher, D.; Davis, L.C. Benzotriazoles: Toxicity and degradation. In Proceedings of the 1998 Conference on Hazardous Waste Research, Snowbird, Utah, 18–21 May 1998; pp. 374–382.
45. Hartwell, S.I.; Jordahl, D.M.; Evans, J.E.; May, E.B. Toxicity of aircraft de-icer and anti-icer solutions to aquatic organisms. *Environ. Toxicol. Chem.* **1995**, *14*, 1375–1386. [CrossRef]
46. Trček, B.; Žigon, D.; Kramarič Zidar, V.; Auersperger, P. Profiles of the benzotriazole pollutant transformation products in an urban intergranular aquifer. *Water Res.* **2018**, *144*, 254–264. [CrossRef]
47. Yang, C.; Dong, W.; Cui, G.; Zhao, Y.; Shi, X.; Xia, X.; Tang, B.; Wang, W. Highly efficient photocatalytic degradation of methylene blue by P2ABSA-modified TiO_2 nanocomposite due to the photosensitization synergetic effect of TiO_2 and P2ABSA. *RSC Adv.* **2017**, *7*, 23699–23708. [CrossRef]
48. Ohsada, T.; Izumi, F.; Fyiki, Y. Raman Spectrum of Anatase, TiO_2. *J. Raman Spec.* **1978**, *7*, 321–324. [CrossRef]
49. Mandić, V.; Plodinec, M.; Kerekovic, I.; Juraic, K.; Janicki, V.; Gracin, D.; Gajović, A.; Mogus-Milankovic, A.; Willinger, M.G. Tailoring anatase nanotubes for the photovoltaic device by the anodization process on behalf of microstructural features of titanium thin film. *Sol. Energy Mater. Sol. Cells* **2017**, *168*, 136–145. [CrossRef]